Iraqi Journal of Science, 2025, Vol. 66, No. 1, pp: 409-422
DOI: 10.24996/ijs.2024.65.1.32

ISSN: 0067-2904

# Creating Landslide Susceptibility Map Using Pairwise Comparison Model in Soran City, Irbil Province, Iraq

**Ahmed Amer[*1], Mufid alhadithi[1], Muntather Aidi shareef[2]**
[1]*Engineering technical college-Baghdad*
[2]*Engineering technical college- Kirkuk*

Received: 14/9/2022 Accepted: **5**/1/2024 Published: 30/1/2025

**Abstract**

Landslide susceptibility maps are essential for planning and dealing with natural disasters in mountainous areas. Soran City, Iraq, was selected to use pairwise comparison models to produce the landslide area's susceptibility map. Three data sources were used to create a landslide inventory map: a satellite image, a field investigation, and previous studies. The satellite image utilized in this investigation is LANDSAT-8, downloaded from the USGS website, consisting of 11 bands with 16-days and 30 m temporal and spatial resolutions, respectively. Consequently, 72 landslides were identified and mapped, with 53 (70%) chosen randomly to create the landslide susceptibility model and the remaining 19 (30%) used to validate the models. Eight landslide conditioning factors were studied to build pairwise comparison models to produce a landslide susceptibility map. These factors encompass slope aspect, slope degree, land use, elevation, curvature, NDVI, road distance, and distance to stream. Consequently, the area under the curve (AUC) analysis showed that the measure of the level of disorder in the model with an AUC value of 0.7 has the maximum prediction accuracy at 73.3 %. The susceptibility maps generated by Pairwise comparison models produce an accurate prediction of the susceptibility of the Kamarbandi Soran-Papshtia road segment to landslides, which can be used as a tool for planning land use and reducing disasters.

**Keyword:** GIS Multi-Criteria Analysis, Landslide, Soran, Iraq

# إنشاء خريطة الحساسية للانهيارات الأرضية باستخدام نموذج المقارنة الزوجية في مدينة سوران، محافظة أربيل، العراق

**احمد عامر، مفيد الحديثي[*] ، منتظر عيدي شريف**
الكلية التقنية الهندسية ، بغداد، العراق
الكلية التقنية الهندسية ، كركوك،العراق

**الخلاصه**

تعد خرائط الحساسية للانهيارات الأرضية مهمة للتخطيط والتعامل مع الكوارث الطبيعية في المناطق الجبلية مثل سوران الذي تم اختياره كمنطقة دراسة. في الدراسة الحالية، تم استخدام نماذج المقارنة الزوجية لتحليل قابلية تأثر طريق Kamarbandi Soran Papshtia والمنطقة المحيطة به للانهيارات الأرضية. تم استخدام ثلاثة مصادر بيانات لإنشاء خريطة حصر الانهيارات الأرضية، مثل صورة القمر الصناعي والتحقيق

[*]Email: ahmedaamer119@gmail.com

الميداني والدراسات السابقة. صورة القمر الصناعي المستخدمة في هذا التحقيق هي LANDSAT−8 التي تم تنزيلها من موقع USGS على الويب والتي تتكون من 11 نطاقًا بدقة 16 يومًا و 30 مترًا من حيث الوقت والمكان على التوالي. وبالتالي، تم تحديد 72 انهيارًا أرضيًا ورسم خرائط لها، حيث تم اختيار 53 حالة (70٪) عشوائيًا لإنشاء تصميمات نماذج حساسية للانهيارات الأرضية، وتم استخدام الـ 19 حالة المتبقية والتي تمثل (30٪) لتأكيد النماذج. تمت دراسة ثمانية عوامل تكييف للانهيارات الأرضية في هذه الدراسة لبناء نماذج مقارنة زوجية لإنتاج خريطة قابلية الانهيار الأرضي. تشمل هذه العوامل جانب المنحدر ودرجة الانحدار واستخدام الأرض والارتفاع والانحناء ؛ NDVI. المسافة إلى الطريق والمسافة للتيار. وفقًا للمنطقة الواقعة تحت المنحنى (AUC)، تُظهر النتيجة أن قياس مستوى الاضطراب في النموذج بقيمة AUC تبلغ 0.7 لديه أقصى دقة للتنبؤ عند 73.3 بالمائة. تنتج خرائط الحساسية التي تم إنشاؤها بواسطة نماذج المقارنة الزوجية تنبؤًا دقيقًا لقابلية قطاع طريق Kamarbandi Soran−Papshtia للانهيارات الأرضية، والتي يمكن استخدامها كأداة لتخطيط استخدام الأراضي والحد من الكوارث.

## 1. Introduction

Landslides are geological events that include a wide range of earth motions, rock falls, deep slope collapses, shallow wreckage influx, and other offshore, coastal, and onshore habitats that may be vulnerable to mass movements [1]. Landslides occur due to the force of gravity and elements that may contribute to the original slope settlement. Creating landslide inventory maps requires detecting, identifying, and classifying landslides and many factors that affect them [2]. The main deciding factor in the recognition of landslides is their size; therefore, any landslide hazard assessment must include an assessment of the magnitude and probability of landslide occurrence [3]. Landslide susceptibility is the likelihood of a landslide occurrence in an area based on local terrain conditions [4]. It is the degree to which slope movements can affect terrain, that is, an estimate of ‘‘where’’ landslides are likely to occur. The advent of remote sensing and GIS has made landslide susceptibility mapping easier today. Different methods to prepare landslide susceptibility and hazard maps using statistical methods and GIS tools such as logistic regression (LR) and weights-of-evidence were developed in the last decade [5][6]. Several investigators have proposed other methods, including weighting factors, weighted linear combinations of instability factors [7], landside nominal risk factors [8], and probabilistic-based frequency ratio models. There are some other data mining techniques such as support vector machine [9], decision tree methods [10], spatial decision support system (SDSS) [11], spatial multi-criteria evaluation (SMCE) [9], index of entropy [12], evidential belief function (EBF) [10], etc. to evaluate the landslide susceptibility, to overcome shortcomings in the methods mentioned above. Data used Landsat satellite images, uploaded a picture of the study area, raised 73 coordinates along the study area, and used geological photos of the study area. The study gap is the lack of a good study of the areas and knowledge of the soil quality and geological layers. Through heavy rains, layers and soil disintegrate, which leads to the occurrence of landslides, as well as human factors, such as blocking roads. To solve the problem and reduce landslides, soil nature and the geological layers of any region must be studied. This paper aims to produce a landslide susceptibility map of the Kamarbandi Soran-Papshtia road using the GIS-Based Multi-Criteria Decision-Making (MCDM) technique. These models exploit information obtained from the inventory map to predict where landslides may occur in future areas in northern Iraq; these models are tested, and the results are discussed.

## 2. The study area

A study area is located at 48°E and 36°N latitude and spans 120 km, and the 120 km Kamarbandi Soran-Papshtia road runs through mountainous terrain northeast of Erbil, the capital of the Iraqi Kurdistan region. The study area's minimum and maximum height ranges from 467-2137 m. The geological and morphological characteristics of the study area include

the Zagros orogenic belt, which stretches from southeast Turkey to the south of Iran in a group of mountains ranging between the Alpine and Himalayas, around 2,000 km long.

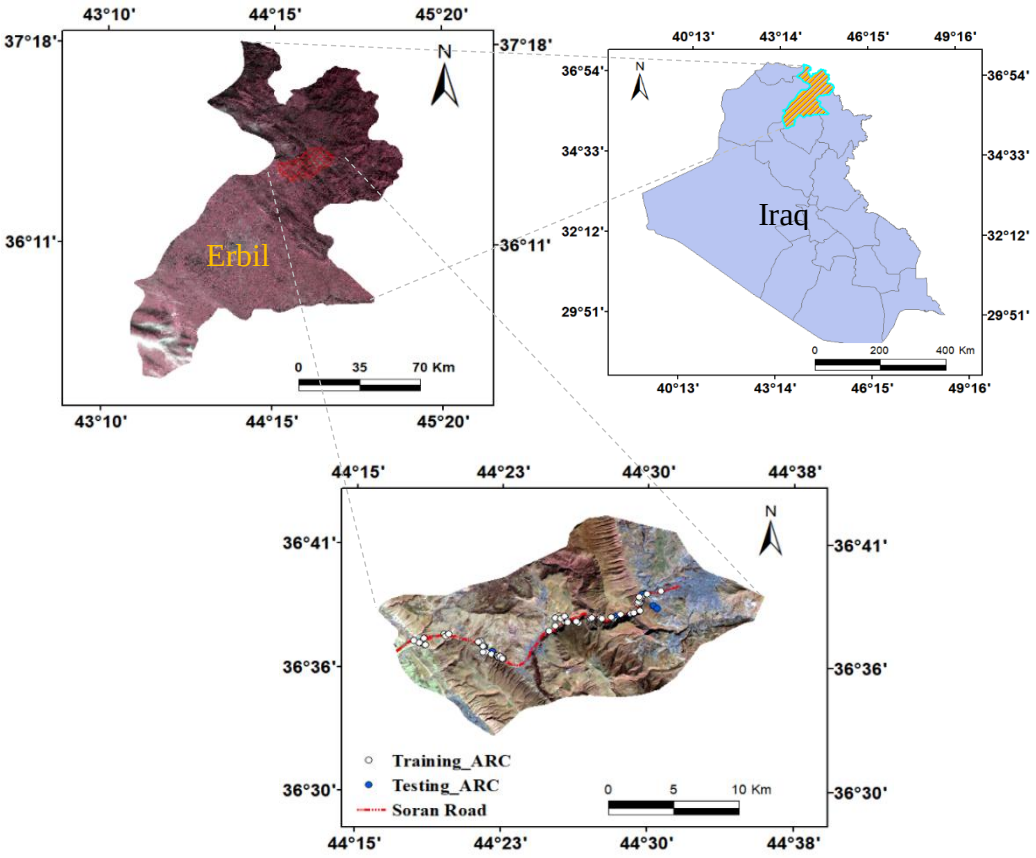


**Figure 1:** Location map of the study area

Iraq is separated into four primary tectonic zones, and each zone has its set of attributes, such as the type of rocks, age, structural evolution, and thickness. The four primary tectonic zones include (1) the Inner platform (stable shelf); (2) the outer platform (unstable shelf), which contains the overlapped zone, the zone of the high fold, the zone of the foothill, and the Mesopotamia fore deep; (3) the Shalair zone; and (4) the Zagros suture zone are including the four zones; Ophiolites are prevalent in the suture zone [11]. The study area comprises ten units produced by the Arabian plate's obduction and collision with the Iranian plate through the Mio-Pliocene and the late Cretaceous periods [13]. Moreover, the Qulqula-Khwarkurk zone, composed of radiolarian cherts, mudstones, limestone, conglomerates, and bare volcanic rocks, is located northeast of the study area. The Penjween-Walash zone is composed of metamorphosed rocks and carbonate beds with volcanic and pyroclastic rocks, and the Shalair zone is composed of meta-pelitic, meta-carbonates, volcanic, and various types (river terraces, alluvial fans, slope sediments, valley fills, flood plains, polygenetic sediments) cover these formations. Triassic to Quaternary alluvial rocks, considered primarily limestone, but include bitumen, marl, siltstone, conglomerate, sandstone, claystone, shale, and dolomite [14]. In most portions of the study region, the terrain is rugged, and the elevations range from 467-2137 m, with slopes ranging from flat to 79 degrees. The combined actions of tectonic uplift, erosion, and varied rock strengths have created this landscape. Severe erosion and moderate weathering created the existing geomorphological units. After being freshly exposed, most of the rocks protruding in the area have a high brightness [15].

The Soran road passes through 12 geological formations, which are: Injana (upper Fars) Formation, Fatha (Lower Fars) formation, Pilaspi Formation, Avanah Formation, Shiranish Formation, Aqra-Bekhme Formation (locally with Kometan Formation), Qamchuqa formation, Balambo, Garagu and Sarmord formations, Tanjero Formation, Slope deposits. The geological layer through which Soran Road passes is the Shiranish Formation, Figure (2) [16].

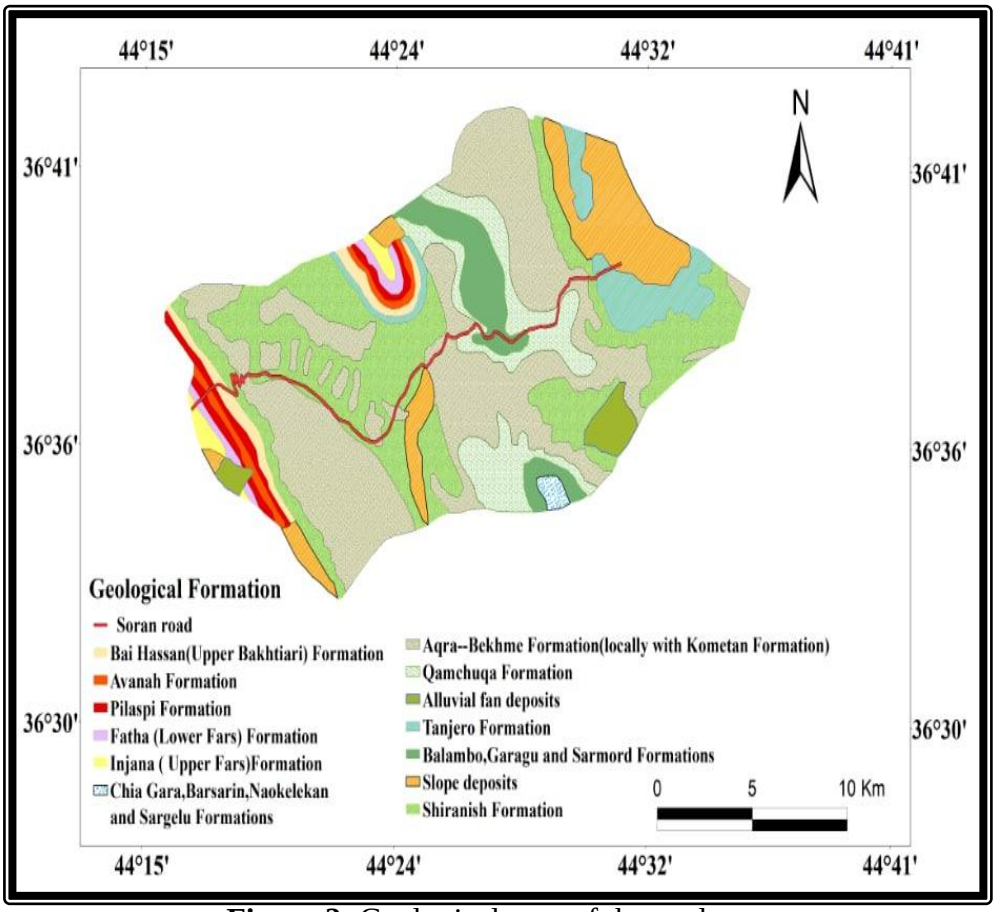


**Figure 2:** Geological map of the study area

## 3. Classification

It is the process of sorting or arranging entities into groups or categories; on a map, representing group members by the same symbol is usually defined in a legend. Classification was used in ArcGIS, cartography, and remote sensing to generalize complexity and extract meaning from geographic phenomena and geospatial data. There are different kinds of classifications, but all generally involve a classification schema or key, which is a set of criteria (usually based on the attributes of the individuals) for deciding which individuals go into each class. Changing the classification of a data set can create various maps.

## 4. Material and Methods

Figure (3) illustrates the main methodology of this study, represented by data collection, methods, and validation. The LANDSAT-8 satellite imagery, which consists of the 11 bands, Table 1, was used as data. It was acquired and downloaded from the USGS website. The satellite data has 11 bands, each with a 16-day temporal resolution and a 30 m spatial resolution [20], Table 1. Up to 15 m of additional spatial resolution have been achieved using the panchromatic band, or 8-band. Most predicted landslide criteria are essential for slope stability and were divided into three groups by morphological, geological, and environmental aspects, which were developed using these images. The current study used eight variables:

aspect, slope, land use, elevation, curvature, NDVI map, distance to the road, and distance from the stream.

**Table 1:** The band characteristic for Landsat 8 [17].

| Band Number | Band With | Description | Resolution(m) |
|---|---|---|---|
| Band 1 | 0.43-0.45 | Coastal aerosol | 30 |
| Band 2 | 0.45-0.51 | Blue | 30 |
| Band 3 | 0.53-0.59 | Green | 30 |
| Band 4 | 0.64-0.67 | Red | 30 |
| Band 5 | 0.85-0.88 | Near Infrared (NIR) | 30 |
| Band 5 | 1.57-1.65 | SWIR 1 | 30 |
| Band 7 | 2.11-2.29 | SWIR 2 | 30 |
| Band 8 | 0.50-0.68 | Panchromatic | 15 |
| Band 9 | 1.36-1.38 | Cirrus | 30 |
| Band 10 | 10.6-11.19 | Thermal Infrared (TIRS)1 | 100 |
| Band 11 | 11.50-12.51 | Thermal Infrared (TIRS)2 | 100 |

### 4.1. Extracting the Morphometric factors

#### 4.1.1. Slope gradient

The slope gradient map was used in this investigation with a 12.5 cm resolution. As indicated in the figure, the initial slope angle values ranged from 0-79 degrees and were separated into five groups based on the most typical subdivisions (4). In addition, most of the Soran road travels on constant slopes ranging from 0-9, then grows to a maximum slope of roughly 79 in some places.

#### 4.1.2. Slope aspect

The slope factor is crucial in developing maps depicting landslide risk. Physically, the aspect is related to the elements that influence landslides, wind impacts, sun exposure, and precipitation [18]. The slopes of the study area range between 0-79 m with different classes. However, five groups were created from the study area, including the slope's direction. In this study, it should be mentioned that the slope is a direction ranging from west to south, Figure (5).

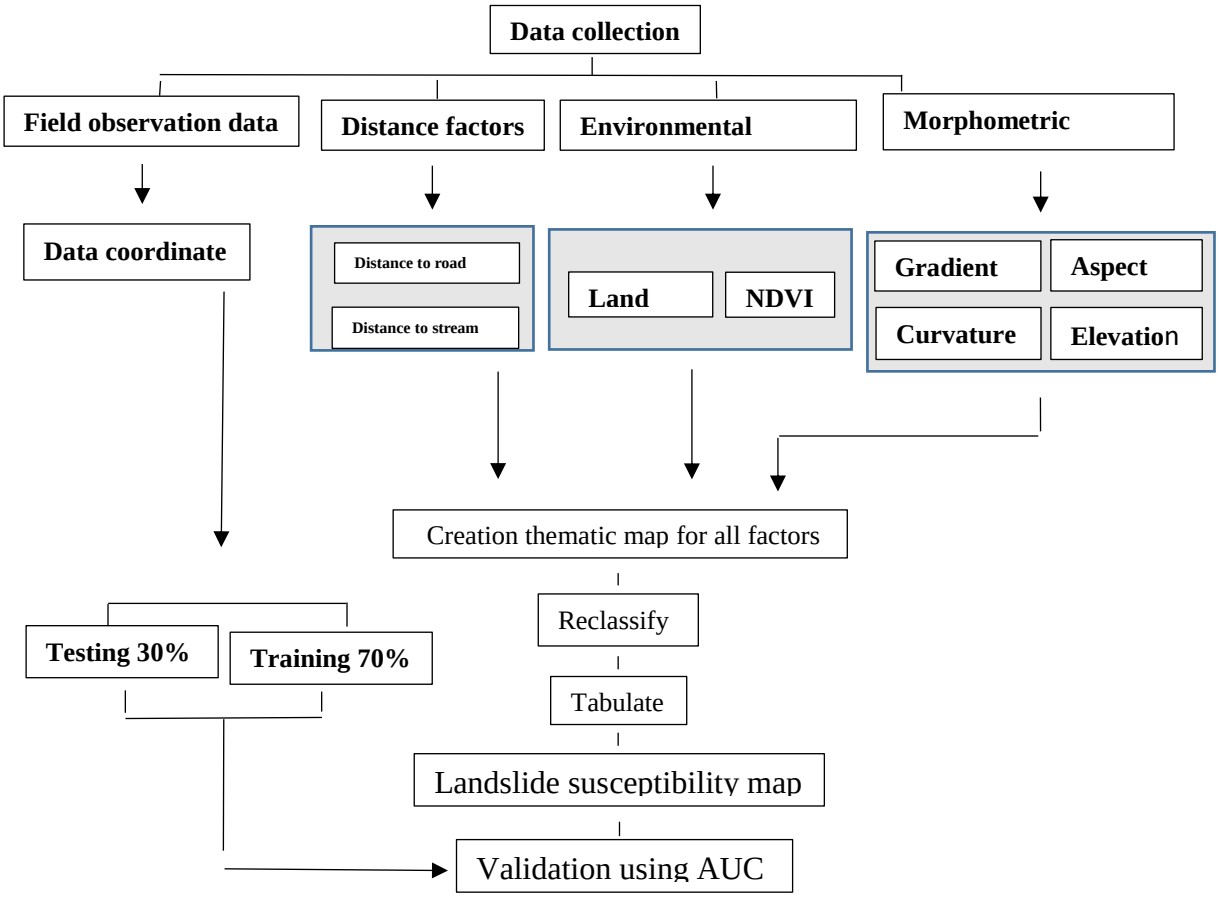


**Figure 3:** Flow chart of the applied method.

### 4.1.3. Land use map

Five different types of land were used in the study area, with most of the land barren. The other four types of land consist of green areas, residential areas, agricultural areas, and water bodies, where most of the road passes in arid areas, Figure (6).

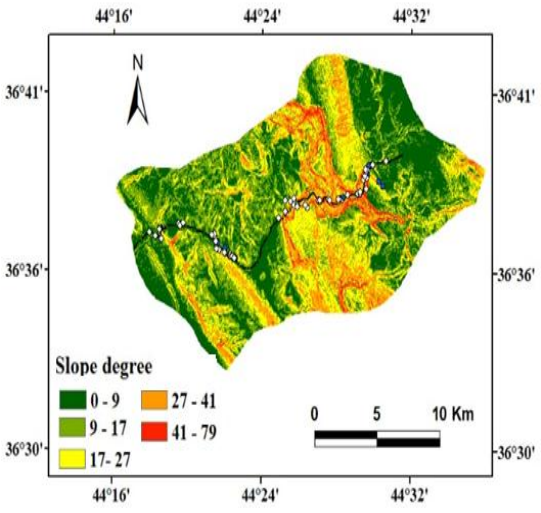


**Figure 4:** Slope gradient map

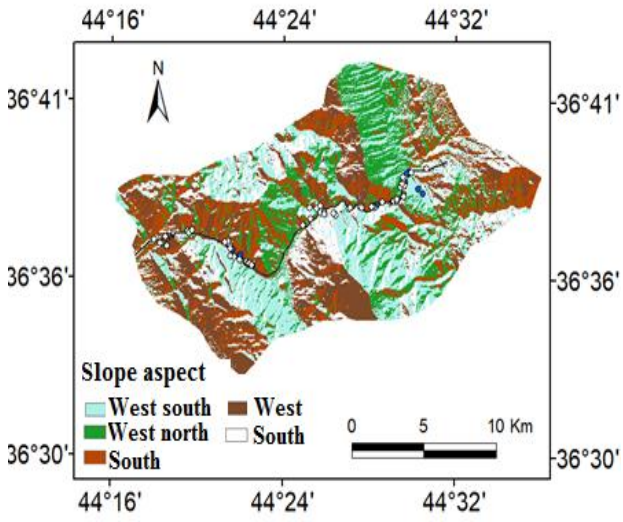


**Figure 5:** Slope aspect map

#### 4.1.4. Elevation

The elevation is considered one of the main factors in studying land sliding; the elevations of the study area range from 467-2137 m and were divided into five groups, Figure (6) based on their heights. The landslide region was close to the road and was separated into two groups. The first group's values range from 762-467, while the second group's values range from 960-762, which reflect the lowest values of the other classes, Figure (7).

#### 4.1.5. Curvature

The surface's curvature refers to the positive or negative values in image data, which means the surface portion has a concave or convex shape. A flat surface was represented by the number 0 [19], whereas a positive value indicated a surface that is convex upwards. A concave-upwards by a negative value, and an upwards by a convex-downwards by a negative value. Five classes were used in this study to describe the curvature status of the study region, with a curvature ranging from 35.84 to 40.32. The bulk of the research region displays a turning state from concave to convex slope in nearly all places; the first two classes ((-35) - (-1)) displayed a concave-upward surface slope. Concavity was represented by the remaining two classes, which ranged from "0.7-40". This represented the concavity according to the resulting values, but it is small, Figure (8).

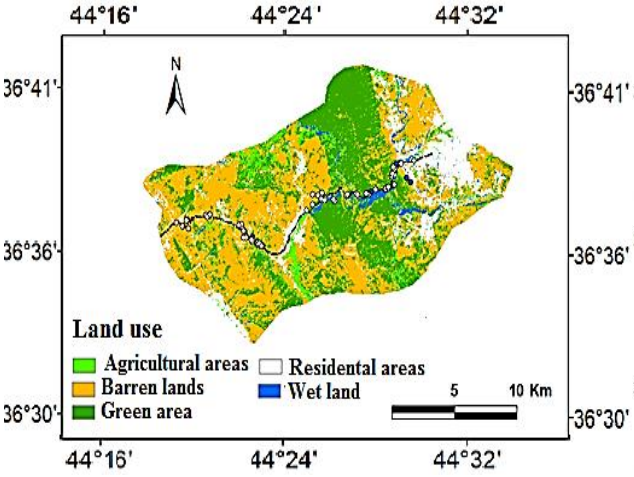


**Figure 6:** Land use map

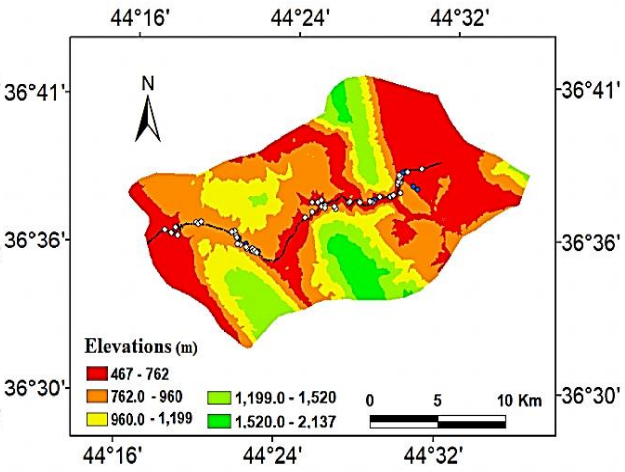


**Figure 7:** Elevation map

### 4.2. Extracting Environmental factors

#### 4.2.1. Normalized Difference Vegetation Index (NDVI)

NDVI is a measure that separates vegetated areas from different classes found in the image data [20]. NDVI values vary from -1 to 1, with a negative value indicating a lack of vegetation or a poor vegetation cover and a positive value indicating a thick, healthy vegetation cover. The research area was classified into five categories to analyze the vegetation status in the area and assess the amount, quality, and density of plant cover, Figure (9), which helped to decrease landslides in the area. It has been noted that the areas around the research sites were characterized by a lack of plant cover, with values ranging from -0.1 to 0.04 comprising weeds.

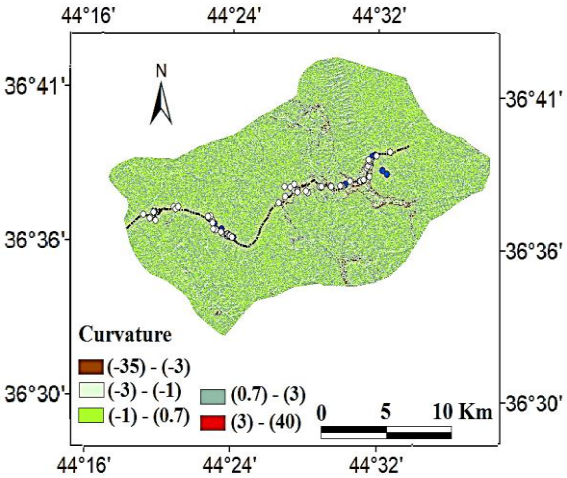


**Figure8:** Curvature map

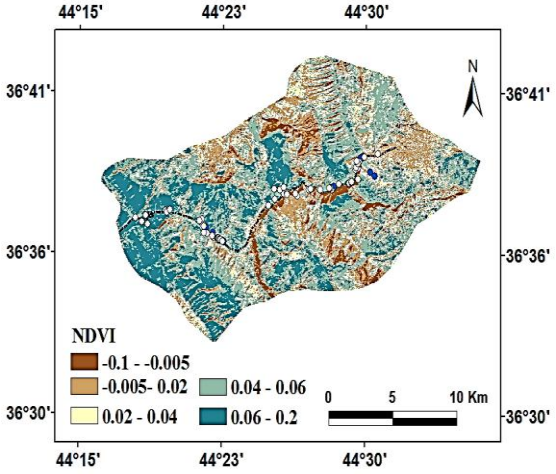


**Figure 9:** NDVI map

### 4.3. Distance factors

#### 4.3.1. Distance from the roads

Changes in the terrain and the lack of support brought on by the building of highways on slopes were the causes of the increase in pressure behind the slope and the development of cracks [21]. A road segment acts as a barrier, net source, net basin, or corridor for water movement. Instabilities could develop in the slope and are typically a cause of landslides. The detailed road network map on the road map was utilized to compute the distance, Figure (10). Regarding the distance from a chart of the road system, the walnut and pink areas were closer to the road network, while the red, green, and light blue areas were farther away.

#### 4.3.2. Distance to the stream

The surface rainfall-runoff flow system erodes the rocks, creating grooves and subsequently generating intermittent streams, which constitute one of the most important reasons influencing the instability of the slope, which causes landslides [22]. Additionally, the farther away from the stream, the greater the likelihood of a landslide. A drainage convergence map was created using Arc GIS 10.8.1, and the slope distance from the stream was divided into five groups, ranging from 200-1200 m, Figure (11), to illustrate the accurate details of the streams toward the road and to discover the main parts of landslide area near the road.

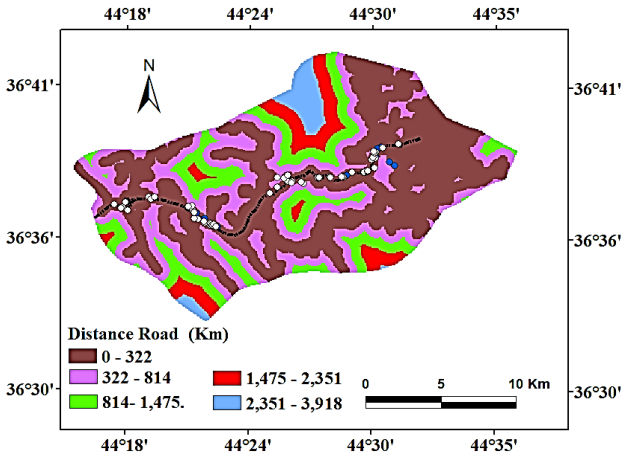


**Figure 10:** Distance to roads

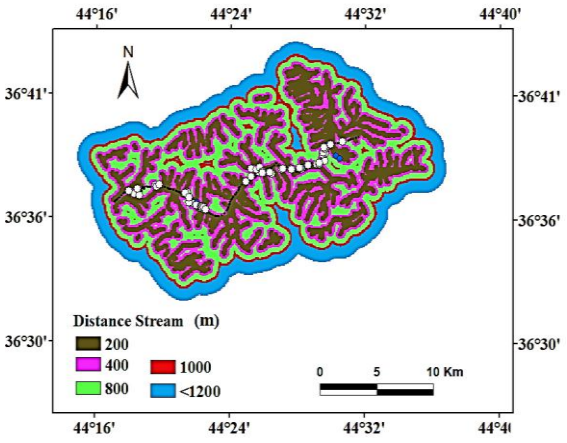


**Figure 11:** Distance to stream

#### 4.3.3. Pairwise comparison

The Pairwise comparison method refers to
any process of comparing entities in pairs. It
considers judging whether each entity was preferred, has a greater amount of some quantitative property, or whether the two entities are identical. The pairwise comparison method was used as a paired comparison in the scientific study of preferences, attitudes, voting systems, social choice, public choice, requirements engineering, multi-agent systems, and psychology literature. It compared the factors in order of preference, the most significant and causing landslides. Moreover, the factors affecting the landslides include Stream power index, slope, distance stream, distance road, land use, elevation, Topographic wetness index, profile, NDVI, curvature, and aspect. The formula for the number of independent pairwise comparisons is represented by:
K (k-1)/2,

Where k is the number of conditions if had three conditions, this would work out as 3(3-1)/2 = 3, and these pairwise comparisons would be gap 1 vs. gap 2, gap 1 vs.
Pairwise comparison extracted the weights of each image reached to predict landslides as in a table. The prediction rate illustrated the factors that have the most influence on the occurrence of landslides and which were possible to detect, analyze, and predict landslides, where the factors that influence a substantial percentage to the least influential factor have been noted. Consequently, if the value was more significant than 1, the landslide ratio was higher than the area when the landslides occurred, indicating a higher correlation, while values less than 1 indicate a lower correlation [23].

## 5. Result and discussion

### 5.1. Landslide Susceptibility Index map

The map was used to evaluate the data compared with landslide site data; the results demonstrated the model's accuracy using the elements that determine how each forecast pattern was rated. The index standards were discovered for each cell in satellite data used in the study region. The produced index was organized in descending order, and the value of each ranking cell was then separated into 100 groups with cumulative one percent intervals, according to Shirzadi et al. (2012) [24]. Thus, the spatial correlation between landslide and conditioning variables was determined using the model values for eight distinct landslide conditioning factors, Table (2).
Pairwise comparison by overlaying and calculating the Pairwise comparison of landslides has created the final landslide susceptibility index (LSI) map. The resulting LSI map was produced using the following equation:

$$LSI = Wm1 + Wm2 + Wm3 + \cdots\cdots + Wmn \quad ,---------- (1)$$

LSI = Landslide susceptibility index; Wm = Weighted thematic maps of conditioning factors. These equations repress the entered factors, which repress the affective factors to produce a suitability map. However, the suitability map showed that the study area was divided into five categories, including safe, low, medium, high, and high, Figure 12. According to the findings, 37 % of the area falls into the very low susceptibility category, with a prediction rate ranging from 1-37. The low susceptibility category was followed by 17%, representing the prediction rate range from 37-54. The medium category represents the area with a prediction rate ranging from 54-67 and 67-80, constituting 13% of the total area of the study area. In comparison, the exceptionally high category constituted 19% ranging between “80 to 100” prediction rate and represents a very active and practical area for landslides and then landslides risk to human life, especially since it was close to the main road.

Consequently, the prediction rates 80-100 were the most vulnerable landslide area hazard occurrence on Soran Road. Consequently, the pairwise comparison model showed that the safe area of landslides was 46.7 $km^2$. The areas that were low susceptibility to the hazards of landslides constitute an area of 65.9 $km^2$. The moderate susceptibility of landslides constitutes an area estimated at 66.3 $km^2$. The high susceptibility of landslides constitutes it, estimated at 55.3 $km^2$. The very high susceptibility of landslides was estimated at 55.22 $km^2$.

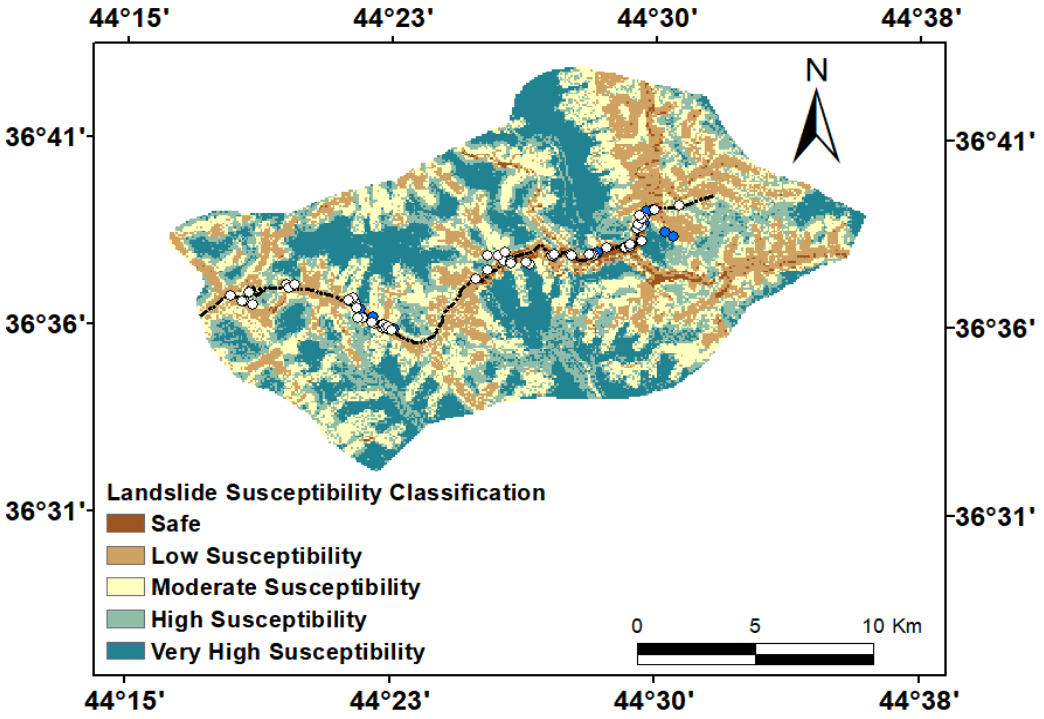


**Figure 12:** The landslide susceptibility map was derived from the Pairwise comparison modal

**Table 2:** Landslide conditioning factors with Pairwise comparison and certainty factor of the landslide

| Factor | Factor classes | No. of point | % of point | Class area | %of class area | Ratio(+) | Model Value |
|---|---|---|---|---|---|---|---|
| *Slope* | 1 | 17600 | 20.3703 | 587732 | 31.8425 | 0.6397 | 0.0657 |
| | 2 | 27200 | 31.4814 | 564801 | 30.6001 | 1.0288 | 0.1057 |
| | 3 | 16000 | 18.5185 | 409516 | 22.1870 | 0.8346 | 0.0857 |
| | 4 | 8000 | 9.25925 | 225589 | 12.2220 | 0.7575 | 0.0778 |
| | 5 | 17600 | 20.3703 | 58109 | 3.14826 | 6.4703 | 0.6649 |
| | | 86400 | 100 | 1845747 | 100 | 9.7311 | 1 |
| *Aspect* | 1 | 14400 | 16.6666 | 361700 | 19.5964 | 0.8504 | 0.1715 |
| | 2 | 14400 | 16.6666 | 356516 | 19.3155 | 0.8628 | 0.1740 |
| | 3 | 28800 | 33.3333 | 390577 | 21.1609 | 1.5752 | 0.3176 |
| | 4 | 14400 | 16.6666 | 367656 | 19.9190 | 0.8367 | 0.1687 |
| | 5 | 14400 | 16.6666 | 369298 | 20.0080 | 0.8329 | 0.1680 |
| | | 86400 | 100 | 1845747 | 100 | 4.9583 | 1 |
| *Land Use* | 1 | 3200 | 3.70370 | 81069 | 6.32766 | 0.5853 | 0.0701 |
| | 2 | 35200 | 40.7407 | 589152 | 45.9849 | 0.8859 | 0.1061 |
| | 3 | 22400 | 25.9259 | 400709 | 31.2764 | 0.8289 | 0.0992 |

| | | | | | | | |
|---|---|---|---|---|---|---|---|
| | 4 | 14400 | 16.6666 | 175900 | 13.7294 | 1.2139 | 0.1454 |
| | 5 | 11200 | 12.9629 | 34353 | 2.68134 | 4.8344 | 0.5790 |
| | | 86400 | 100 | 1281183 | 100 | 8.34862 | 1 |
| *NDVI* | 1 | 8000 | 9.2592 | 72486 | 5.63878 | 1.64206 | 0.31206 |
| | 2 | 9600 | 11.1111 | 200529 | 15.5994 | 0.71227 | 0.13536 |
| | 3 | 14400 | 16.6666 | 335598 | 26.1066 | 0.63840 | 0.12132 |
| | 4 | 40000 | 46.2962 | 392948 | 30.5679 | 1.51453 | 0.28783 |
| | 5 | 14400 | 16.6666 | 283929 | 22.0872 | 0.75458 | 0.14340 |
| | | 86400 | 100 | 1285490 | 100 | 5.26187 | 1 |
| | | 86400 | 100 | 1845747 | 100 | 5.0538 | 1 |
| *Curvature* | 1 | 22400 | 25.9259 | 365901 | 19.7666 | 1.3116 | 0.2643 |
| | 2 | 14400 | 16.6666 | 333521 | 18.0173 | 0.9250 | 0.1864 |
| | 3 | 24000 | 27.7777 | 453466 | 24.4970 | 1.1339 | 0.2285 |
| | 4 | 16000 | 18.5185 | 334202 | 18.0541 | 1.0257 | 0.2067 |
| | 5 | 9600 | 11.1111 | 364016 | 19.6647 | 0.5650 | 0.1138 |
| | | 86400 | 100 | 1851106 | 100 | 4.9613 | 1 |
| *Distance Road* | 1 | 20800 | 24.07407407 | 7505 | 13.4994 | 1.7833 | 0.3941 |
| | 2 | 59200 | 68.5185 | 15974 | 28.7327 | 2.38467 | 0.5270 |
| | 3 | 6400 | 7.40740 | 11557 | 20.7878 | 0.35633 | 0.0787 |
| | 4 | | 0 | 10308 | 18.5412 | 0 | 0 |
| | 5 | | 0 | 10251 | 18.4387 | 0 | 0 |
| | | 86400 | 100 | 55595 | 100 | 4.5243 | 1 |
| *Distance Stream* | 1 | 67200 | 77.7777 | 16952 | 29.0771 | 2.6748 | 0.7197 |
| | 2 | 17600 | 20.3703 | 12366 | 21.2109 | 0.9603 | 0.2584 |
| | 3 | 1600 | 1.8518 | 13272 | 22.7650 | 0.0813 | 0.0218 |
| | 4 | 0 | 0 | 3317 | 5.68953 | 0 | 0 |
| | 5 | 0 | 0 | 12393 | 21.2572 | 0 | 0 |
| | | 86400 | 100 | 58300 | 100 | 3.7165 | 1 |
| *Elevation* | 1 | 38400 | 44.4444 | 371419 | 20.0647 | 2.2150 | 0.4439 |
| | 2 | 19200 | 22.2222 | 372888 | 20.1440 | 1.1031 | 0.2211 |
| | 3 | 28800 | 33.3333 | 369326 | 19.9516 | 1.6707 | 0.3348 |
| | 4 | | 0 | 369096 | 19.9392 | 0 | 0 |
| | 5 | | 0 | 368377 | 19.9003 | 0 | 0 |
| | | 86400 | 100 | 1851106 | 100 | 4.9889 | 1 |

**Table 3:** The area of each class

| Class | The area of each class (Pairwise Comparison) $km^2$ |
|---|---|
| 1 | 46.69 |
| 2 | 65.91 |
| 3 | 66.33 |
| 4 | 55.29 |
| 5 | 55.22 |

## 6. Validation of landslide susceptibility map

The produced landslide susceptibility map (LSI) was validated using the success rate curve, where the LSI map's index values for each pixel were determined. According to the validation results, 70% of pixels were accurately categorized as landslide pixels.

The prediction rate showed the factors that have the most influence on the occurrence of landslides, and then it was possible to detect, analyze, and predict landslides. Moreover, the result revealed that the turbulence level measure for the model with an AUC of 0.7 has a maximum prediction accuracy of 73.3, where the area under the curve was 41.27%, Figure (13).

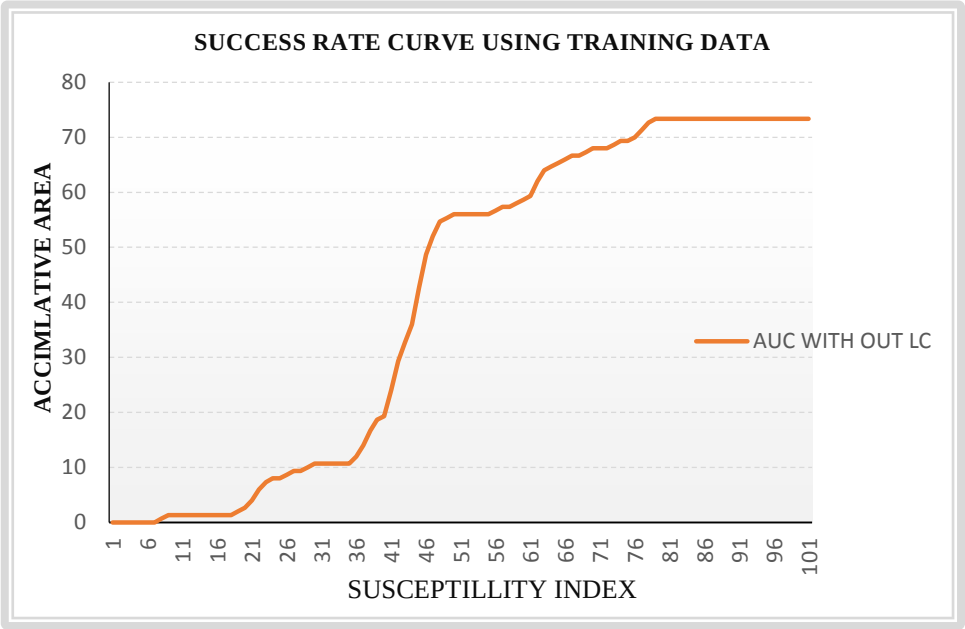


**Figure 13:** Prediction rate curve evaluation of the Pairwise comparison model method

## Conclusions

Producing land sliding suitability maps is one of the most critical issues in evaluating and studying natural hazards in specific areas. A pairwise comparison model was used in Soran Road and its surroundings to evaluate and predict the landslide hazard; eight landslide conditioning factors (aspect, slope, land use, elevation, curvature, NDVI map, distance to road, and distance from stream) were applied for this purpose. The landslide inventory map was created using aerial photos, satellite images, and a comprehensive field survey. Seventy-two landslides were found and mapped. The data were divided into 53 representations (70%) and randomly chosen to create a landslide sensitivity model, and the remaining 19 representations (30%) were used to validate the model.

The susceptibility map was created with the highest accuracy of mortality (73.33%), according to the AUC charts, and the highest value (AUC) (0.7). This showed that all of the models used in this study had a respectable level of accuracy when predicting landslide vulnerability for the Soran Road section. Due to mounting population pressure, people were forced to concentrate their efforts on the rocky mountain slopes. Sensitivity maps can thus be utilized as crucial tools in managing the land and planning upcoming construction projects in this area to protect people and property from landslides. High susceptibility and very high vulnerability areas necessitate additional geological and engineering geotechnical considerations, whereas areas of low sensitivity were considered relatively safe for infrastructure development. Resulting sensitivity maps can be used as part of land

management and planning for future development initiatives in this area to protect people and property from landslides as part of land management and planning for future development initiatives in this area.

**References**


**[1]** E. Derbyshire., "Geological hazards in loess terrain, with particular reference to the loess regions of China." *Earth-Science Reviews*, vol. 54, no. (1-3), pp.231-260, 2001.

**[2]** C. J. Van Westen, T. W. Van Asch, R. Soeters., "Landslide hazard and risk zonation why is it still so difficult." *Bulletin of Engineering Geology and the Environment*, vol.65, no.2, pp.167-184., May 2006.

**[3]** O. Hungr. "A review of landslide hazard and risk assessment methodology" *in Landslides and engineered slopes*, S. Avera, L. Cascini, L. Picarelli, and C. Scavia, CRC Press T&F, 2016 pp.3-25.

**[4]** Clark, C.C., Brabb, E.E., Greene, H.G., Ross, D.C. "Geology of Point Reyes Peninsula and implications for San depressions, Gregorio fault history. In: Crouch, J.K., Bachman, and S.B. (Eds.) Tectonics and Sedimentation along the California Margin. Pac. Sect. Soc. Econ. Palaeontol. Mineral. vol. 38, pp.67-86, April 18-21, 1984.

**[5]** C. J. van Westen, N. Rengers, R. Soeters, R. "Use of geomorphological information in indirect landslide susceptibility assessment." *Natural hazards*, vol. 30 no.3, pp.399-419, 2003.

**[6]** C. Chung, A. Fabbri. "Probabilistic prediction models for landslide hazard mapping." Photogrammetric engineering and remote sensing, vol.65 no. (12), pp.1389-1399, 1999.

**[7]** S. Saha, D. Chant, J. Welham, J McGrath. "A systematic review of the prevalence of schizophrenia." PLOS MEDICINE, vol. 2, no.5, e141. 2005.

**[8]** H. Hong, C. Xu, I. Revhaug and D. Tien Bui. "Spatial prediction of landslide hazard at the Yihuang area (China): a comparative study on the predictive ability of backpropagation multi-layer perceptron neural networks and radial basic function neural networks," In Cartography-maps connecting the world, pp. 175-188. Springer, Cham. January 2015.

**[9]** J. Sui, W. C. Hwang, S. Perez, Ge Wei, D. Aird, et al., "Structural and functional bases for broad-spectrum neutralization of avian and human influenza A viruses." *Nature Structural and molecular biology*, vol. 16, no. 3, pp. 265-273, 2009.

**[10]** A. Naghibi, H. R. Pourghasemi, Z. Pourtaghi, A. Rezaei. "Groundwater qanat potential mapping using frequency ratio and Shannon's entropy models in the Moghan watershed, Iran." *Earth Science Informatics*, vol. 8 no.1, pp. 171-186. 2015.

**[11]** O. F. Althuwaynee, B. Pradhan, S. Lee. "Application of an evidential belief function model in landslide susceptibility mapping. *Computers & Geosciences*, vol. 44, pp.120-135, 2012.

**[12]** M. Mohammady Pourghasemi H. R., B. Pradhan. "Landslide susceptibility mapping at Golestan Province, Iran: a comparison between frequency ratio, Dempster–Shafer, and weights-of-evidence models." *Journal of Asian Earth Sciences*, vol. 61, pp. 221-236, 2012.

**[13]** M., Zainy, N., Al-Ansari, T., Bauer, and M. Ask."The tectonic and structural classifications of the Western part of the Zagros Fold and Thrust Belt, North Iraq, review and discussion." *Journal of Earth Sciences and Geotechnical Engineering*, vol.7, no.2, pp. 71-89, 2017.

**[14]** P., Agard, J. Omrani, L. Jolivet, F. Mouthereau. "Convergence history across Zagros (Iran): constraints from collisional and earlier deformation." *International Journal of Earth Sciences*, vol. 94, no.3, pp. 401-419, 2005.

**[15]** M. F. Coffin, P. D. Rabinowitz. "Evolution of the conjugate East African-Madagascan margins and the western Somali Basin," *Geological Society of America*, vol. 226. 78pp, 1988.

**[16]** R. H. Jahns. "Sheet structure in granites: its origin and use to measure glacial erosion in New England." *The Journal of Geology*, vol.51, no.2, pp.71-98, 1943.

**[17]** T. D. Acharya. I. Yang. Exploring Landsat 8 ." International Journal of IT, *Engineering and Applied Sciences Research*, vol.4, pp.4-10, 2015.

**[18]** Z. Shao, J. Cai, P. Fu, L. Hu, T. Liu. "Deep learning –based fusion of Landsat-8 and Sentinel-2 images for a harmonized surface reflectance product". *Remote Sensing of Environment*, vol. 235, 111425, 2019.

**[19]** K. C., Devkota, A. D., Regmi, H. R., Pourghasemi, K., Yoshida, B., Pradhan, I. C., Ryu, O. F. Althuwaynee. "Landslide susceptibility mapping using certainty factor, index of entropy, and

logistic regression models in GIS and their comparison at Mugling–Narayanghat road section in Nepal Himalaya." *Natural hazards*, vol. 65, no.1, pp.135-165, 2013.

**[20]** A. Schneider. "Monitoring land cover change in urban and peri-urban areas using dense time stacks of Landsat satellite data and a data mining approach." *Remote Sensing of Environment*, vol.124, pp.689-704, 2012.

**[21]** M. A., Lefsky, W. B., Cohen, S. A., Acker, G. G., Parker, T. A., Spies, D Harding. "Lidar remote sensing of the canopy structure and biophysical properties of Douglas-fir western hemlock forests." *Remote sensing of environment*, vol.70, no.3, pp. 339-361, 1999.

**[22]** J. Q. Zhuang, J. B. "Peng. A coupled slope cutting—a prolonged rainfall-induced loess landslide: a 17 October 2011 case study". *Bulletin of Engineering Geology and the Environment*, vol.73, no.4, pp. 997-1011, 2014.

**[23]** H. T. Nguyen, T. Wiatr, T. M. Fernández-Steeger, K. Reicherter, D. M. Rodrigues, R. Azzam. "Landslide hazard and cascading effects following the extreme rainfall event on Madeira Island (February 2010)". *Natural hazards*, vol. 65, no.1, pp.635-652, 2013.

**[24]** A. Shirzadi, L. Saro, O. Hyun Joo, K. Chapi. "A GIS-based logistic regression model in rock-fall susceptibility mapping along a mountainous road: Salavat Abad case study, Kurdistan, Iran." *Natural hazards*, vol.64. No. 2, pp.1639-1656, 2012.